EISCAT SCIENTIFIC ASSOCIATION

**EISCAT
TECHNICAL
NOTE**

**Use of the EISCAT radar as a
supplement to rocket measurements**
by
Kristen Folkestad

**KIRUNA
Sweden**

USE OF THE EISCAT RADAR AS A SUPPLEMENT TO ROCKET MEASUREMENTS

by

Kr. Folkestad
EISCAT
N-9027 Ramfjordmoen
Norway

USE OF THE EISCAT RADAR AS A SUPPLEMENT TO ROCKET

MEASUREMENTS

by

Kr. Folkestad

1 INTRODUCTION

The versatility of the incoherent scatter technique in
ionospheric research is well proven. In conjunction with
rocket borne measurements it can be used in various ways,
for instance as a surveillor to determine suitable launch
conditions, or, during the rocket flight, as a timed moni-
tor of regions physically associated with the rocket sur-
roundings, but remote enough from the trajectory to ensure
that the radar antenna does not see the vehicle.

The feasability of using the radar in a local sensing mode,
to explore the ionosphere in the vicinity of the rocket is
less evident, first of all due to the disturbing influence
of the returns from the rocket body. The difficulties are
further aggravated if the objective is to use the radar to
trace the changes taking place in the medium around a rocket
carrying active experiments. Problems to be considered here
are the extent of the disturbed region, the strength of the
perturbation and its relaxation time as compared with the
time needed for integration of the radar returns. In part
these subjects still seem to be a matter conjecture and
discussions.

With our present knowledge it appears premature to expect
that we can predict, with a reasonable degree of certainty,

the signatures that the actively induced perturbations will leave on the scattered signals. It will be worthwhile, though, to try to define the problem areas as they relate to the particulars of the scatter radar technique. The ballistics of the flying rockets are known with sufficient accuracy to allow a numerical assessment of their imprints on the scattered returns.

This report is concerned with the prospect of using the EISCAT radar in the local surveillance mode in supplementing rocket observations. Within the EISCAT reaches there are two rocket ranges, ESRANGE in Sweden and ANDØYA, Norway. The present note will be restricted to a study of rockets launched from ANDØYA, as observed from the EISCAT station at Ramfjordmoen, near Tromsø.

Before proceeding with the main topic we first briefly describe the characteristics of the EISCAT-system and present some basic features of incoherent scatter observations.

THE EISCAT-SYSTEM

A schematic layout of the EISCAT scatter radar facility presently under installation in North Scandinavia is given in the first figure.
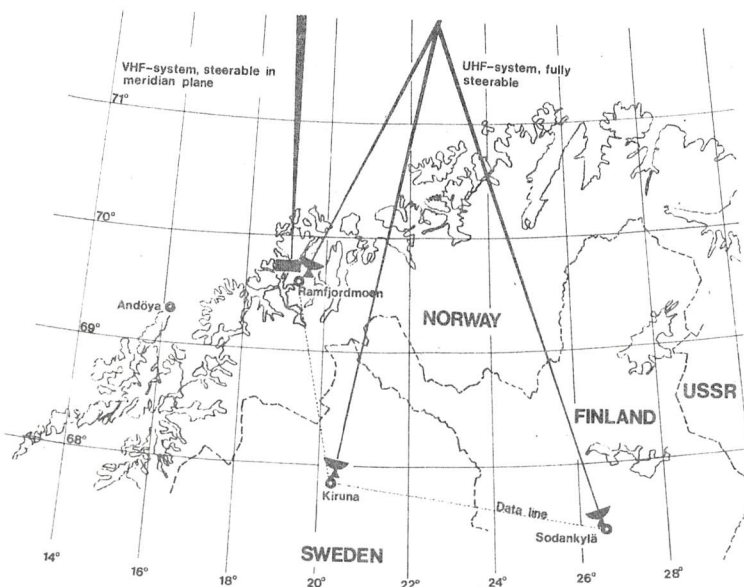

Figure 1   Sketch map of the EISCAT Observatory

The Observatory includes two independent radars, a <u>mono-static</u> VHF-system operating at a centre frequency of 224 MHz, and a <u>tristatic</u> UHF-radar with a centre frequency of 933.5 MHz. The monostatic element uses a 5000 m^2 antenna, shaped as a parabolic cylindre, mechanically movable from 30° south to 60° north of zenith in the meridian plane. The tristatic system has fully steerable parabolic antennae of a diameter 32 m. Since the steering flexibility inherent in the UHF-radar makes this more suitable for rocket-coordinated experiments, we will only deal with this system in the following.

Characteristics of the UHF-radar:

Peak power rating	2.0 MW
Average power	250 kW
Pulse length	10 us - 10 ms
Pulse repetition rate	0-1000 Hz
Modulation waveforms	Single- and multi-pulse, frequency hopping, 13 bits Barker code

Antenna:

Half-power beam width	0.6°
Gain	48 dB
Speed of movement, azimuth and elevation	80°/m

The receiver system employs helium-cooled parametric pre-amplifiers. System noise temperatures are around 40 K for the remote sites and estimated to be about 90 K for the transmitter site. Execution of experiments will take place under computer control, facilitating quick and easy swapping of operational programmes. At the remote stations (Kiruna and Sodankylä) the height of the sampled region will be given by the interception of the antenna beams. At the transmitter station the possibility exists for dividing the returns into a series of range gates, allowing for simultaneous processing of several height intervals.

2   BASICS OF INCOHERENT SCATTER OBSERVATIONS

We might envisage the thermally induced inhomogeneities in the ionospheric electron density distribution as caused

by density waves travelling in all directions with a con-
tinuous distribution of wavelengths. A scatter radar acts
as a spectrum analyzer, picking out those spectral compo-
nents which satisfy the Bragg's reflection condition.

Power spectrum   Autocorrelation function
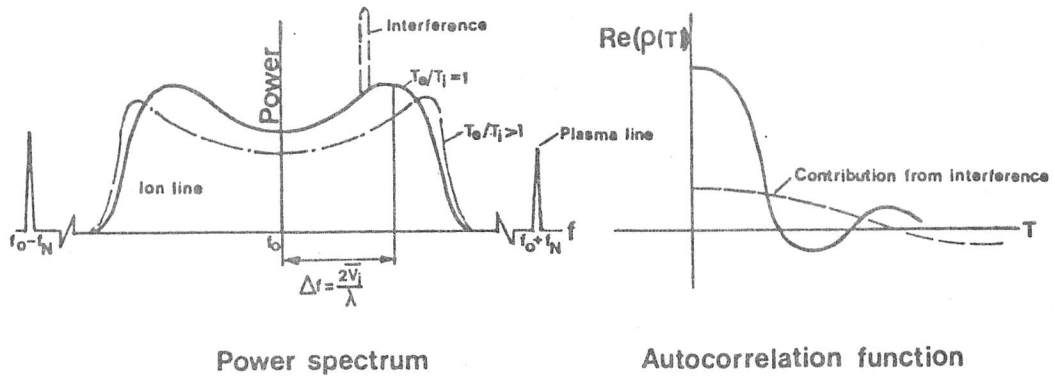
Figure 2   Schematic display of scatter power spectrum
             and real part of autocorrelation function.

The major part of the returned energy, contained in the
socalled ion-line, may be ascribed to ion-accoustic waves
created by the Coulomb forces acting between the electrons
and the ions. Much weaker returns occur in the spectrum at
frequencies displaced from the transmitted frequency by
approximately the ionospheric plasma frequency. These are
termed plasma-lines and may be attributed to electronic
oscillations caused by the repellent force which the elec-
trons exert on each other.

The ion-line generally has a double-humped shape, the
elevation of the shoulders above the central part of the
spectrum being dependent upon the ratio T_e/T_i. As indica-
ted in the figure the distance between the shoulder maxima
(for $T_e = T_i$) is:

$$\Delta f = \frac{2\overline{v_i}}{\lambda} = \frac{4}{0.3} \left(2\frac{kT_i}{m_i}\right)^{\frac{1}{2}} = 1.7 \left(\frac{T_i}{M_i}\right)^{\frac{1}{2}} \text{ kHz} \tag{1}$$

where we have inserted the actual UHF-wavelength. The ion
and electron temperatures will be derived from the ion-line
by adjusting parameters in a theoretical model.

The power associated with the plasma lines is very much smaller than that in the ionic component. A requirement for their observation is the presence of fast electrons, created by: (i) photoionization (Yngvesson and Perkins, 1968), (ii) auroral particles (Kofman and Wickwar, 1980) or, (iii) strong HF-waves (Kantor, 1974). Energies likely to be of importance for the EISCAT UHF-system are in the range 0.5 to 5 eV.

Since the ionospheric scattering result from thermal movements, the information-carrying signals have a noise-like character and, in general, an integration process is needed to enable worthwhile information to be extracted from the measured data. The integration time needed depends upon the wanted accuracy, pulse length, pulse repetition frequency, the noise properties of the system, power output, antenna gain, along with the electron density and the electron- and ion temperatures.

A symmetric ion-line results if the ionosphere is stationary. A doppler displacement of the whole spectrum indicates a drift of the scattering medium. With three stations the drift vector may be determined unambigously.

In an approximate fashion the integrated spectrum relates in a simple way to the ionospheric electron density. Instead of observing the spectrum directly the EISCAT system will measure its Fourier transform, the signal's autocorrelation function. By recording both amplitude and phase of the signal the real as well as the imaginary part of the autocorrelation function are obtained. A symmetric spectrum yields a vanishing imaginary component. An asymmetric spectrum, for instance created by an ionospheric drift or an interferring signal, as indicated in figure 2, will give rise to a nonzero imaginary correlation function component. Note that the total returned power is specified by the zerolag autocorrelation.

The EISCAT Observatory will be provided with a programmable correlator operating at a sampling frequency of 5 MHz (complex samples). The integration time may be set at will and the possibility exists for dividing the integration period into subintervals, transfer of data from the correlator to the computer being effected by the end of each subinterval. In addition, at the Tromsø station, there will be a French multi-bit correlator capable of sampling at rates as high as 15 MHz. This latter unit is particularly suited for measurements of plasma lines.

3. ROCKET-COORDINATED MEASUREMENTS

3.1 Geometry and trajectories

Three different rocket trajectories are sketched in figure 3. The ones at 0° and 340° azimuth are considered as possible launch options for POLAR 6, a Norwegian-Austrian-US venture, designed to carry a 10 keV electron accelerator into the auroral ionosphere. The trajectory at 35° azimuth refers to a rocket termed HERO, to be flown through a region modified by an HF heating wave from the Max-Planck facility at Ramfjordmoen. In the following discussion we will deal primarily with problems pertinent to POLAR 6. Several of the features brought forth will be common, though, to all rockets launched from Andøya, for which local scatter radar surveillance is desirable.

The distance Ramfjordmoen-Andøya is 130 km. Slant range distances from the UHF-antenna to four points on the 0°-trajectory are indicated, for instance, the distance from the antenna to the downleg trajectory point at 100 km altitude is 237 km.

Estimated apogees for the POLAR 6 and HERO trajectories are about 206 and 275 km respectively. The statistical

uncertainty, given in terms of standard deviations, amounts to $\pm$ 5 km for the apogee and 15 km for the impact area (Haugen, private communication). For the rocket distances indicated in figure 3 the lateral dimension of the main beam is in the range 1.5 to 2.5 km. Without attempting to transfer the statistical uncertainties in the trajectory descriptions into the antenna's reference system, it is clear that with an antenna programmed to follow a predertermined path there is a substantial risk that the rocket will not appear within the view of the main lobe. The uncertainty in this respect will be largest for the descent protion of the flights. Work is going on (Haugen, private communication) to establish a system where the rocket coordinates are determined at the rocket range in an online fashion by combining the settings of the s-band telemetry antenna with slant range information. Should this attempt be successful, the possibility exists for improving the pointing accuracy of the EISCAT antennae by remote control.
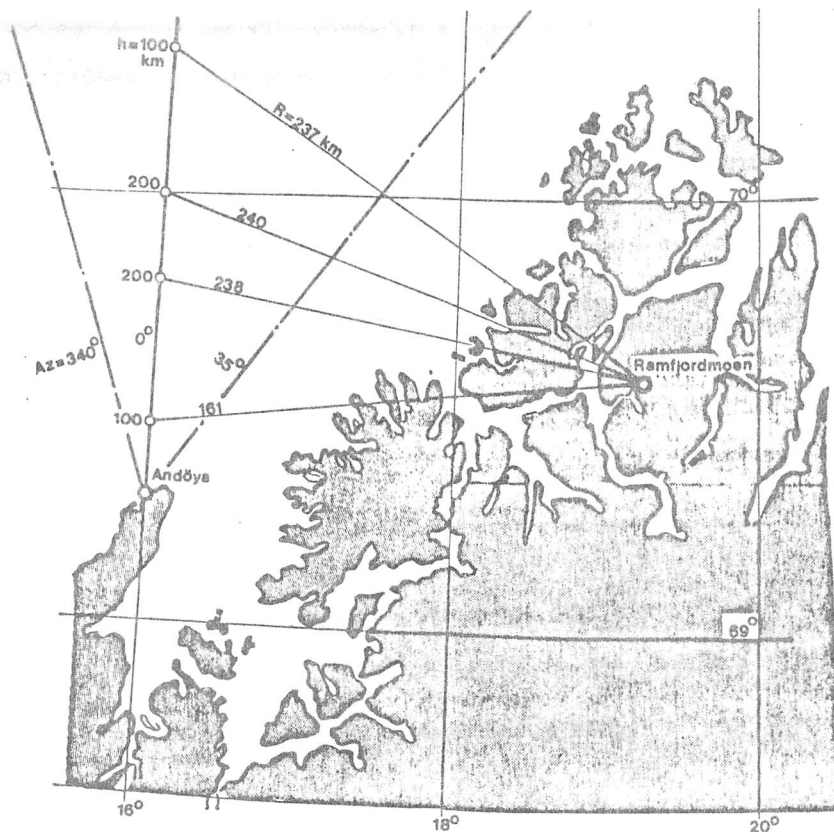
Figure 3   Launch directions and EISCAT geometry

3.2 Cross sections

The cross section of the POLAR 6 rocket, in a plane
through its axis, is close to 1.5 m^2. As viewed from
the EISCAT site during the flight the rocket projection
is likely to be less. However, it is a common experience
that sounding vehicles at times exhibit unpredictable
coning motions where almost any position is possible.
For comparing the returns from the rocket with those
from the ionospheric target it seems reasonable to assume
a radar cross section of 1 m^2.

Using radar theory as applied to incoherent scatter (ionos-
phere) and "hard target" reflections (rocket) we derive
the approximate formula for the ratio of the instantaneous
powers returned from the rocket and from the surrounding
medium:

$$P_r/P_s = \frac{4A\sigma \text{ rocket } (1 + T_e/T_i)}{\lambda^2 R^2 c\sigma_o \tau N_e} \qquad (2)$$

where A is the effective area of the antenna, R denotes
slant range, c is the velocity of light, τ the pulse length,
N_e electron density and σ_{rocket} and σ_o the rocket cross
section and Thomson's cross section of an electron ($=10^{-28}$ m^2).
By inserting actual values for the constants and variables
we find a power ratio in the range $10^6 - 10^8$. P_r ranges
from 10^{-9} to 10^{-10} watt, which is well below the saturation
level (-40 dB$_m$) of the forefront receiver.

With the filters/attenuators set for reception of scatter
signals from the background plasma it appears that the
rocket returns are bound to saturate stages in the receiver
chain following the preamplifier. The question which arises
is whether some suitable method may be devised for discrimi-
nating the unwanted signal. We will return to this problem
later in the report.

3.3 Beam crossing

Figure 4 shows the antenna polar diagram as measured for
the horizontal polarization. With the power ratio from
the preceding section in mind it is evident that the rocket
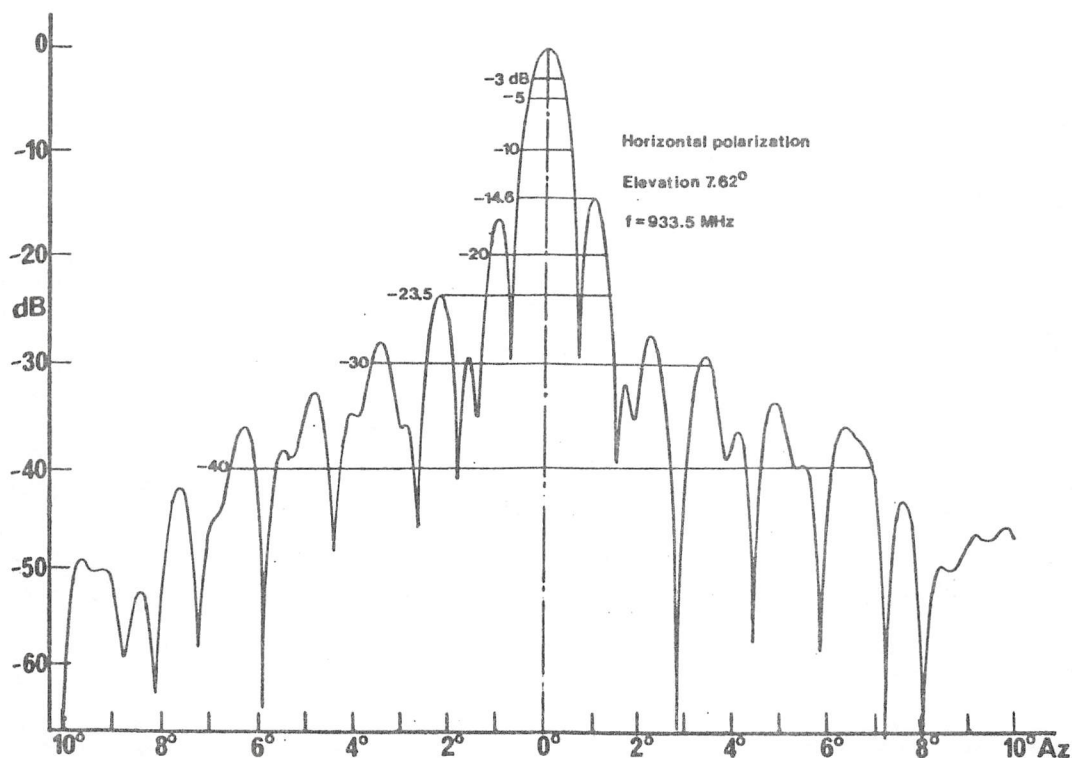will be observed far out in the side-lobe structure.

Figure 4   Antenna polar diagram for horizontal
polarization

To estimate the time needed for the rocket to traverse
the antenna pattern at the different levels the following
procedure has been adopted: From the trajectory specifi-
cations the position coordinates versus time are known.
An accompanying programme has been constructed (Haugen,
pricate communication) to give the elevation, φ, and
azimuth, Φ, of the radar antenna for an arbitrary point
on the trajectory. The computations have been carried out
in the following steps: (i) The antenna has been set to
intercept the rocket trajectory at a point defined by t_o,

φ_O and Φ_O. (ii) For a time interval including t_O the elevation and azimuth angles for the rocket pointing directions have been noted. For a particular time t_1 the angle between the pointing direction and the antenna axis is given by the formula:

$$\cos\Delta\alpha_1 \;=\; \cos\varphi_1 \, \cos\varphi_O \, \cos(\Phi_1 - \Phi_O) + \sin\varphi_1 \, \sin\varphi_O \qquad (3)$$
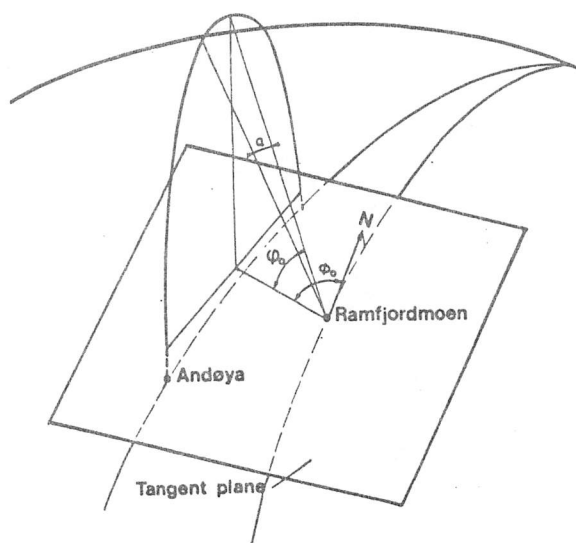

Figure 5   Geometry used for beam crossing computations

By repeating the procedure for other trajectory points a series of pairs Δt ($= t - t_O$) and $\Delta\alpha$ has been formed. Figure 6 has been established by relating the angular deviations, $\Delta\alpha$, to the damping levels in figure 4.

For a given dB-level in figure 6 the ordinate specifies the time which elapses from the first instance the rocket experiences a relative radiation above the level considered to the instance the intensity drops below this level for the last time. As will be noted from figure 4 the time interval defined in this way might span short intermediate drops corresponding to the minima between side lobes.
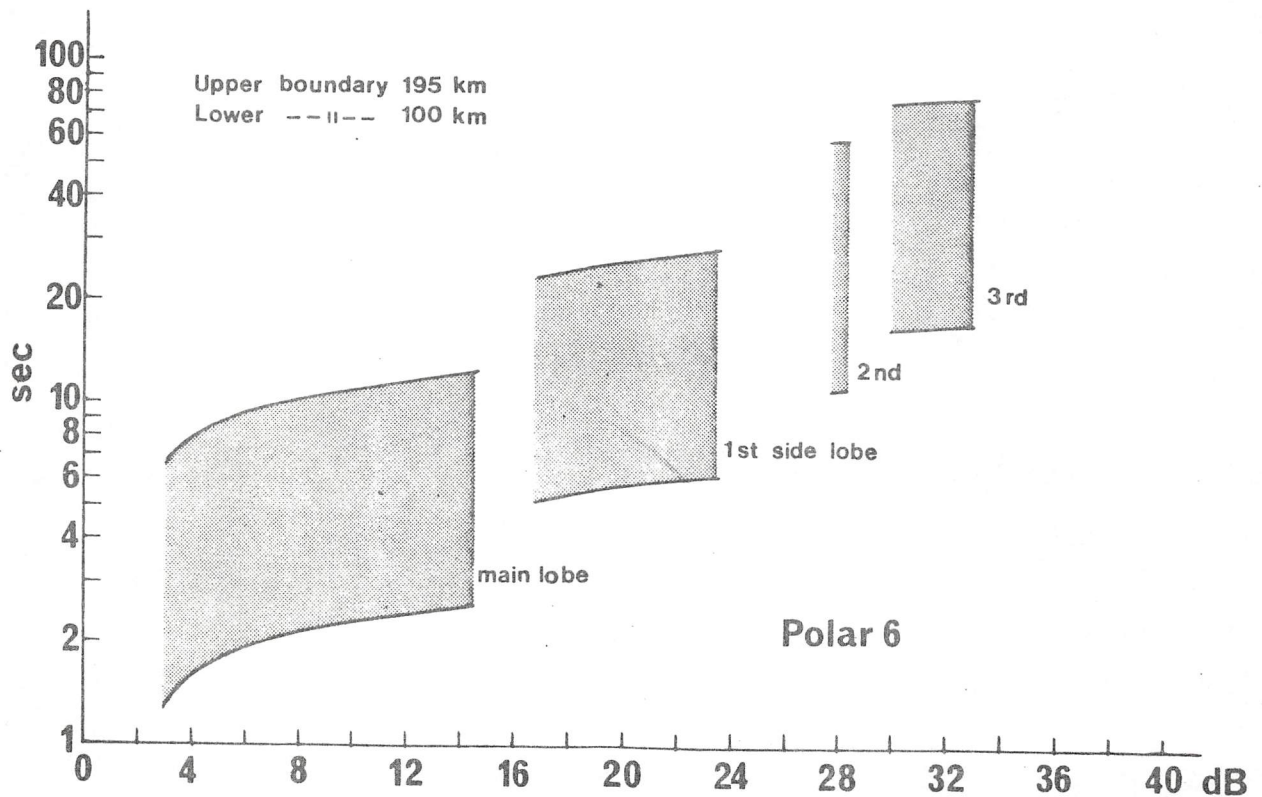
Figure 6   Beam crossing time as function of relative
            damping in antenna polar diagram

The computations have been performed for two reference
height levels, 100 and 195 km. The "beam passing time" is
found to increase very notably as the rocket velocity falls
with increasing height. For the selected references the
difference in passing times amounts almost to a factor of 5.
A marked dependence upon the selected dB-level is also
noted. We will return to the consequences of this relation-
ship in the later discussion.

3.4 Doppler displacements of rocket reflections

Figure 7 and 8 show the doppler displacements to be
expected for the signals reflected by the rocket bodies,

computed by the formula:

$$\Delta f \quad = \quad \frac{2v_r}{\lambda} \tag{3}$$

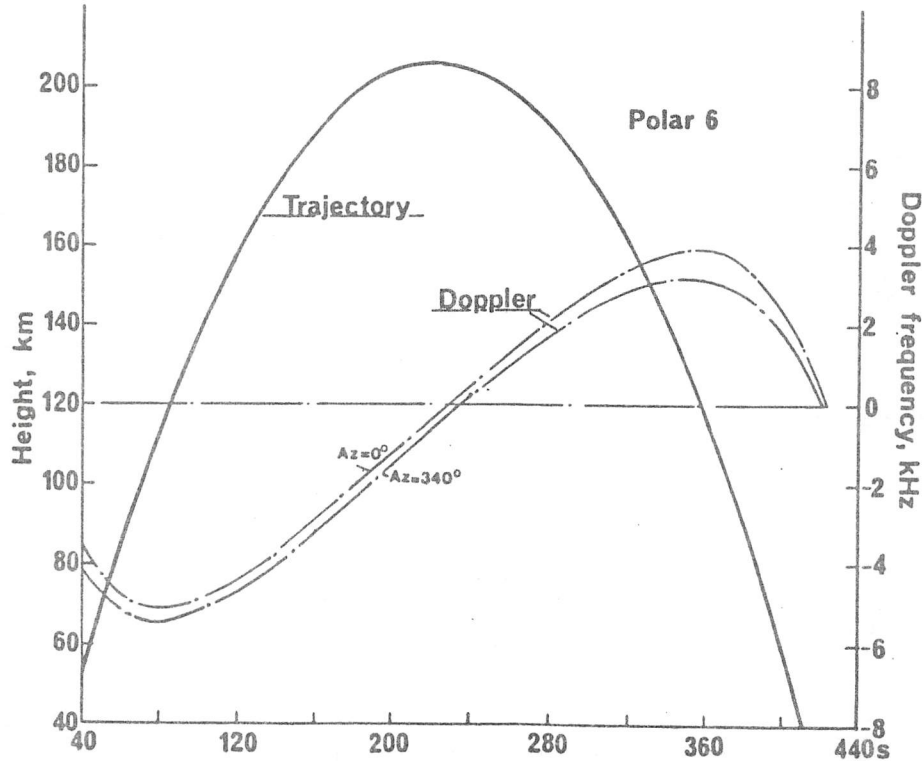where v_r is the radial velocity as seen from Ramfjordmoen.

Figure 7   Doppler displacements of signals reflected from POLAR 6
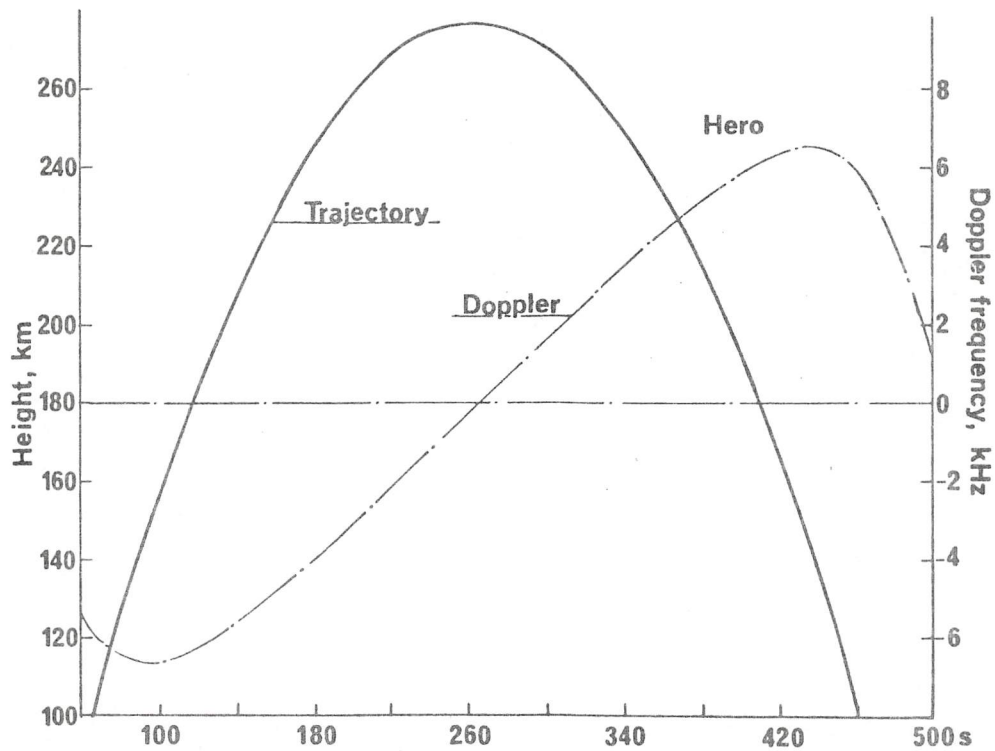

Figure 8   Doppler displacements of signals reflected from HERO

The doppler frequencies are found to reach values in the range 5-6 kHz, changing from negative to positive as the rocket's radial velocities reverse not far from the apogees.

3.5 Integration times and statistical uncertainties

As mentioned before the information carrying signals have a noisy character and their observation is heavily influenced by the noise behaviour of the receiving system.

The signal-to-noise ratio, essential in determining the relative uncertainty of the measurements, depends upon the selection of modulation waveform. Apart from Barker-coded signals the EISCAT modulation repertoire includes single- and multi-pulse schemes. The latter option uses repeated bursts of short, unequally spaced, pulses, particularly well suited for good spatial resolution. It is believed that the multi-pulse waveform will be of special interest for the local surveillance case considered in this report.

Estimates made for a 5-pulse group (Williams, EISCAT/SAC document 17.17) for ranges and parameters actual for the EISCAT radar and the rocket experiments studied here, give integration times in the range 100-150 sec for a statistical uncertainty of 5%, 10 μs pulse lengths and a PRF (rather pulse burst frequency) of 100. By increasing the PRF to 300 the integration times drop by a factor of 3. For 10% uncertainty and a PRF of 300, maintaining the pulse length, the integration times are in the range 8-12 s. The integration times referred to are relatively insensitive to changes in N_e or the T_e/T_i-ratio.

It is possible to decrease the integration periods further by increasing the pulse lengths, but this can only be done at the expence of reduced spatial resolution. The range resolution is given be $\Delta h = c\tau/2$, and amounts to 1.5 km for PL = 10 μs.

It may be possible, within the duty cycle constraints
of the transmitter (12.5%), to operate with somewhat
higher PRF-rates than quoted above. The possibility also
exists for reducing the number of pulses in the group.
It is conceivable, therefore, to achieve integration time
of the order of a few seconds, provided the need for a
very good accuracy is relaxed.

3.6 Plasma-lines

According to theory Landau damping and ion-electron col-
lisions are expected to limit the observations of plasma
lines to plasma frequencies in the range

$$2/\lambda < f_N < 6/\lambda \tag{4}$$

which for the EISCAT UHF radar corresponds to

$$6 < f_N < 18 \text{ MHz}$$

There is experimental evidence, however, that the detecta-
bility range predicted by (4) is too narrow. For the
Chatanika radar relation (4) gives a lower limit for
f_N of about 8 MHz, yet Kofman and Wickwar (1980) have
reported on plasma line observations with the same radar
at plasma frequencies as low as 3 MHz.

We shall not here discuss the problem of extracting physical
parameters from plasma line measurements, just mention that
electron densities may be readily derived since the fre-
quencies at which they are observed closely approximate
the plasma frequencies in the generation regions. The pos-
sibility also exists for determining electron temperatures
from plasma line observations (Hagfors and Lehtinen, 1981).
The literature describes several types of instabilities
involved in the evolution of plasma line oscillations (e.g.
see, Fejer, 1979). Of particular interest in our context

may be observations made under conditions where the
plasma lines are enhanced by HF radio waves (Ganguly,
1980). It is claimed that under such circumstances the
line intensities may be enhanced as much as 10^5 above
the thermal level. For such high intensities an integration
time of 0.1 s has been found to be adequate.

A more detailed discussion of the possibility of observ-
ing plasma-lines generated by artificial electron beams
in the ionosphere would have to address topics such as:
(i) electric fields generated and how they relate to
the thresholds for the various plasma line instabilites,
(ii) what is the level and life time of electron density
enchancements created by beam plasma interactions in the
various energy ranges, (iii) the spatical extent of the
disturbances as compared with the volume of the sampled
background plasma and, (iv) propagation direction of en-
hanced density waves relative to the direction of the
exploring scatter radar beam.

A thorough treatment is bound to become complicated. Under
the circumstances it seems advicable to adopt the prag-
matic attitude of attempting to observe any signatures
of the modification first and then, should the outcome be
positive, search for an explanation afterwards.

3.7 Discussion and summary

This note has addressed the possibility of using the
EISCAT radar at Ramfjordmoen to monitor the ionosphere
in the immediate surroundings of rockets launched from
Andöya. Although the treatment has been restricted to
two rocket flights, the conclusions reached should be
valid for other rocket flights as well. Moreover, the
slant ranges (referred to Ramfjordmoen) for rockets
launched from ESRANGE, Kiruna, are comparable with those

for the Andöya launches. This indicates that our results should apply, at least in an approximate fashion, also for rockets flown from Kiruna.

In the following we try to summarize our findings:

- The statistical uncertainty inherent in any prede-termined trajectory specification implies that there is a substantial risk that the main lobe of the radar antenna will miss the rocket, or that the rocket may appear in the main lobe in cases when one deliberately tries to avoid this. Adequate pointing accuracy, there-fore, seems to require online steering possibility.

- The rocket cross sections are expected to vary over a wide range, but may yield returns as much as 70-80 dB above the background level.

- While the rocket reflections are not likely to saturate the preamplifiers, they are expected to do so for the subsequent receiver chain, unless they can be appropri-ately filtered.

- For actual ion compositions and temperatures the ion-line is likely to require a filter bandwidth of 15-20 KHz. For all types of rockets the doppler displacements of the returns will be within the ion-line filter bandwidth. For ion-line diagnostics this reduces the possibility of discriminating against the rocket reflections by a filtering technique. The prospect of applying program-mable filters appears to be complicated enough to render the possibility hardly worthwhile trying.

- The very notable disparity in the cross sections of the rockets and the background plasma indicates that even for a vehicle in a remote sidelobe the rocket returns may be detrimental. An estimate of the "beam crossing times" demonstrates that several tens of

seconds will have to elapse before the rockets have
receded so far out that sensible ion-line measurements
can be made. It is unlikely that disturbances created
by active in situ experiments will have a comparable
life time.

- For plasma-line observations the rocket returns can be
  filtered out an are therefore expected to cause no
  serious problems. Whether in active rocket experiments
  the plasma lines are excited to a level permitting de-
  tection remain basically uncertain. Joint experiments
  may provide the answer. There is experimental evidence
  that powerful HF waves may cause a drastic enhancement
  of plasma line intensities. For the HERO-rocket, which
  is to measure through a region "heated" in this way,
  the prospect should be promising for observing the lines
  concerned.

References

Fejer, J A — Rev Geophys and Space Phys 17, 135 (1979)

Ganguly, S — J Geophys Res 85, 1783 (1980)

Hagfors, T and M Lehtinen — J Geophys Res 86, 119 (1981)

Kantor, I J — J Geophys Res 79, 199 (1974)

Kofman, W and V Wickwar — J Geophys Res 85, 2998 (1980)

Williams, P J S — SAC document 17.17 (1980)

Yngvesson, K O and F W Perkins — J Geophys Res 73, 97 (1968)

EISCAT publications

F. du Castel, O. Holt, B. Hultqvist, H. Kohl and M. Tiuri:
A European Incoherent Scatter Facility in the Auroral Zone (EISCAT).
A Feasibility Study ("The Green Report") June 1971. (Out of print).

O. Bratteng and A. Haug:
Model Ionosphere at High Latitude, EISCAT Feasibility Study, Report
No. 9.
The Auroral Observatory, Tromsö July 1971. (Out of print).

A European Incoherent Scatter Facility in the Auroral Zone, UHF
System and Organization ("The Yellow Report"), June 1974.

EISCAT Annual Report 1976.(Out of print).

P.S. Kildal and T. Hagfors:
Balance between investment in reflector and feed in the VHF cylindri-
cal antenna.
EISCAT Technical Notes No. 77/1, 1977.

T. Hagfors:
Least mean square fitting of data to physical models.
EISCAT Technical Notes No. 78/2, 1978.

T. Hagfors:
The effect of ice on an antenna reflector.
EISCAT Technical Notes No. 78/3, 1978.

T. Hagfors:
The bandwidth of a linear phased array with stepped delay corrections.
EISCAT Technical Notes No. 78/4, 1978.

Data Group meeting in Kiruna, Sweden, 18-20 Jan. 1978
EISCAT Meetings No. 78/1, 1978

EISCAT Annual Report 1977

H-J. Alker:
Measurement principles in the EISCAT system
EISCAT Technical Notes No. 78/5, 1978

EISCAT Data Group meeting in Tromsö, Norway 30-31 May, 1978
EISCAT Meetings No. 78/2, 1978.

P-S. Kildal:
Discrete phase steering by permuting precut phase cables.
EISCAT Technical Notes No. 78/6, 1978

EISCAT UHF antenna acceptance test.
EISCAT Technical Notes No. 78/7, 1978.

P-S. Kildal:
Feeder elements for the EISCAT VHF parabolic cylinder antenna.
EISCAT Technical Notes No. 78/8, 1978.

H-J. Alker:
Program CORRSIM: System for program development and software
simulation of EISCAT digital correlator, User's Manual.
EISCAT Technical Notes No. 79/9, 1979.

H-J. Alker:
Instruction manual for EISCAT digital correlator.
EISCAT Technical Notes No. 79/10, 1979

H-J. Alker:
A programmable correlator module for the EISCAT radar system.
EISCAT Technical Notes No. 79/11, 1979.

T. Ho and H-J. Alker:
Scientific programming of the EISCAT digital correlator.
EISCAT Technical Notes No. 79/12, 1979.

S. Westerlund (editor):

Proceedings EISCAT Annual Review Meeting 1969. Part I and II,

Abisko, Sweden, 12-16 March 1979.

EISCAT Meetings No. 79/3, 1979.

J. Murdin:

EISCAT UHF Geometry.

EISCAT Technical Notes No. 79/13, 1979.

T. Hagfors:

Transmitter Polarization Control in the EISCAT UHF System.

EISCAT Technical Notes No. 79/14, 1979.

B. Törustad:

A description of the assembly language for the EISCAT digital

correlator.

EISCAT Technical Notes No. 79/15, 1979.

J. Murdin:

Errors in incoherent scatter radar measurements.

EISCAT Technical Notes No. 79/16, 1979.

EISCAT Digital Correlator. TEST MANUAL.

EISCAT Technical Notes No. 79/17, 1979.

G. Lejeune:

A program library for incoherent scatter calculation.

EISCAT Technical Notes No. 79/18, 1979.

K. Folkestad:

Lectures for EISCAT Personnel, Volume I

EISCAT Technical Notes No. 79/19, 1979.

Svein A. Kvalvik:

Correlator Buffer-Memory for the EISCAT Radar system

EISCAT Technical Notes. No. 80/20.

P-S. Kildal:
EISCAT VHF Antenna Tests
EISCAT Technical Notes No. 80/21

J. Armstrong:
EISCAT Experiment Preparation Manual
EISCAT Technical Notes No. 80/22

A. Farmer:
EISCAT Data Gathering and Dissemination
EISCAT Technical Note 80/23

Terrance Ho and Hans-Jørgen Alker:
Scientific Programming of the EISCAT Digital Correlator (Revised)
EISCAT Technical Note 81/24

Terrance Ho:
Programs Corrsim, Corrtest: System for Program Development and
Software Simulation of EISCAT Digital Correlator. User s manual.
EISCAT Technical Note 81/25

Terrance Ho:
Instruction Manual for EISCAT Digital Correlator (Revised).
EISCAT Technical Note 81/26

Terrance Ho:
Standard Subroutines and Programs for EISCAT Digital Correlator.
EISCAT Technical Note 81/27

Terrance Ho:
Pocket Manual for Programming the EISCAT Digital Correlator.
EISCAT Technical Note 81/28

K, Folkestad:
Lectures for EISCAT Personnel, Volume II,
EISCAT Technical Note 81/29

M, Lehtinen och Anna-Liisa Turunen:
EISCAT UHF antenna direction calibration
EISCAT Technical Note 81/30